



CHORUS

This is the accepted manuscript made available via CHORUS. The article has been published as:

Preferential Rotation of Chiral Dipoles in Isotropic Turbulence

Stefan Kramel, Greg A. Voth, Saskia Tymphel, and Federico Toschi

Phys. Rev. Lett. **117**, 154501 — Published 5 October 2016

DOI: [10.1103/PhysRevLett.117.154501](https://doi.org/10.1103/PhysRevLett.117.154501)

Preferential rotation of chiral dipoles in isotropic turbulence

Stefan Kramel and Greg A. Voth*
*Department of Physics, Wesleyan University,
Middletown, Connecticut 06459, USA*

Saskia Tjempel
*Department of Applied Physics,
Eindhoven University of Technology,
5600 MB, Eindhoven, The Netherlands*

Federico Toschi[†]
*Department of Applied Physics and Department of Mathematics and Computer Science,
Eindhoven University of Technology,
5600 MB, Eindhoven, The Netherlands
and
Istituto per le Applicazioni del Calcolo,
Consiglio Nazionale delle Ricerche,
Via dei Taurini 19, 00185 Rome, Italy*

(Dated: August 30, 2016)

We introduce a new particle shape which shows preferential rotation in three dimensional homogeneous isotropic turbulence. We call these particles chiral dipoles because they consist of a rod with two helices of opposite handedness, one at each end. 3D printing is used to fabricate these particles with length in the inertial range and their rotations are tracked in a turbulent flow between oscillating grids. High aspect ratio chiral dipoles preferentially align with their long axis along the extensional eigenvectors of the strain rate tensor, and the helical ends respond to the extensional strain rate with a mean spinning rate that is non-zero. We use Stokesian dynamics simulations of chiral dipoles in pure strain flow to quantify the dependence of spinning on particle shape. Based on the known response to pure strain, we build a model that gives the spinning rate of small chiral dipoles using velocity gradients along Lagrangian trajectories from high resolution direct numerical simulations. The statistics of chiral dipole spinning determined with this model show surprisingly good agreement with the measured spinning of much larger chiral dipoles in the experiments.

An incompressible turbulent fluid flow produces exponential stretching of material line segments. In 1952, Batchelor conjectured that this must occur [1], and subsequent work has confirmed his conjecture, determining that their average exponential growth rate is $\zeta = \langle e_i S_{ij} e_j \rangle \approx 0.12 \tau_\eta^{-1}$, where S_{ij} is the strain rate tensor, τ_η the Kolmogorov time, and e_i is the orientation unit vector for the material line [2–4]. One might wonder how an incompressible flow can stretch material lines on average since every fluid element must combine extension with contraction to maintain constant volume. The answer lies in the Lagrangian advection of material lines which causes them to preferentially orient along extensional directions of the velocity gradient tensor.

The rate of separation of two material points is the longitudinal velocity difference, Δu_r . Randomly sampled points have $\langle \Delta u_r \rangle = 0$ due to incompressibility. To obtain insights into the dynamics of turbulence from longitudinal velocity differences at random orientations, one needs to consider higher moments. For example, the third moment in the inertial range is related to the mean energy dissipation rate by Kolmogorov’s 4/5 law:

$\langle (\Delta u_r)^3 \rangle = -\frac{4}{5} \langle \epsilon \rangle r$. However, two points advected by the flow develop a preferential orientation. In this oriented Lagrangian reference frame, the mean velocity difference is positive; in particular, for small r the mean velocity difference is $\langle \Delta u_r \rangle / r = \zeta$.

The study of stretching of material elements has led to many insights into the dynamics of turbulence. Many studies since Richardson have explored two particle dispersion, focusing on the rate of separation of two particles that are initially close together [5]. The ‘advected delta-vee’ system [6, 7], in which velocity differences are sampled between two points advected in the flow but constrained to maintain fixed distance, has illuminated the development of intermittency in turbulent flows. The positive mean stretching rate of vorticity in turbulence has been shown to result from vorticity becoming aligned with the extensional directions of the velocity gradient tensor [8–10].

Recently there has been extensive research on the dynamics of rigid non-spherical particles in turbulent fluid flows [11–14]. Connections between particle dynamics and fluid stretching suggest that non-spherical particles

may be able to provide revealing probes of fundamental processes in turbulent flows [15].

In this letter, we introduce a new particle design that responds to stretching with a preferential rotation **in homogeneous, isotropic turbulence**. Measuring rotations of these particles with multiple high speed cameras allows us to experimentally observe the mean stretching experienced by orientable elements in turbulent fluid flows. The particle has two helical ends with opposite handedness as shown in Fig. 1(a). We call these particles chiral dipoles because of their similarity to electrical dipoles. The total chirality of the particle is zero; however, the two ends with opposite chirality are separated by a fixed distance. The chiral dipole vector, \hat{d} , points from the right-handed end to the left-handed end. A similar particle design was mentioned by Purcell [16], predicting that such a particle would sink through a quiescent fluid without spinning.

When placed in a pure strain flow, a high aspect ratio chiral dipole like the one shown in Fig. 1(b) tumbles until \hat{d} points along the extensional strain direction. The strain flow then couples to the chiral dipole shape to produce a solid body rotation rate in the direction of the chiral dipole vector, $\Omega = \Omega_d \hat{d}$, where Ω_d is called the spinning rate. **In a turbulent flow, the particle becomes aligned by the strain, and experiences $\langle \Omega_d \rangle > 0$ due to the persistence of strain along \hat{d} . Preferential rotation requires isotropy to be broken. Although the flow is isotropic on average, instantaneous flow structures are strongly anisotropic due to the stretching they have experienced. We show that carefully designed particles can couple to this local anisotropy to allow preferential rotation.**

We use Stokesian dynamics simulations [17] to quantify the rotational motion of chiral dipoles in a pure strain flow in order to help choose the shapes to fabricate. A complex shaped particle like a chiral dipole can be modeled with individual spheres, each fixed in their relative position as shown in Fig. 1(a). **The model is allowed to rotate freely while it is subjected to constant velocity gradients. The particle shape can be specified by the pitch of the helices and the aspect ratio, $\alpha = l/D$, where l is the length of the particle and D is the diameter of the helices. The pitch is defined as the length along the helix axis for a complete turn divided by D . We know the particle should have a high aspect ratio, $\alpha \gg 1$ to ensure good alignment with the extensional eigenvectors of the strain rate tensor [12].**

Figure 1(c) and (d) show the mean spinning rate from the Stokesian dynamics simulations of chiral dipoles in a two-dimensional pure strain flow with strain rate eigenvalues $\lambda_1 = -\lambda_3$ and $\lambda_2 = 0$. After an initial orientation phase of 5 to 10 times the characteristic strain rate time scale (λ_1^{-1}), the particle aligns with the extensional eigenvector of the strain rate tensor and begins to spin about its long axis at a rate Ω_d , with the mean value calculated

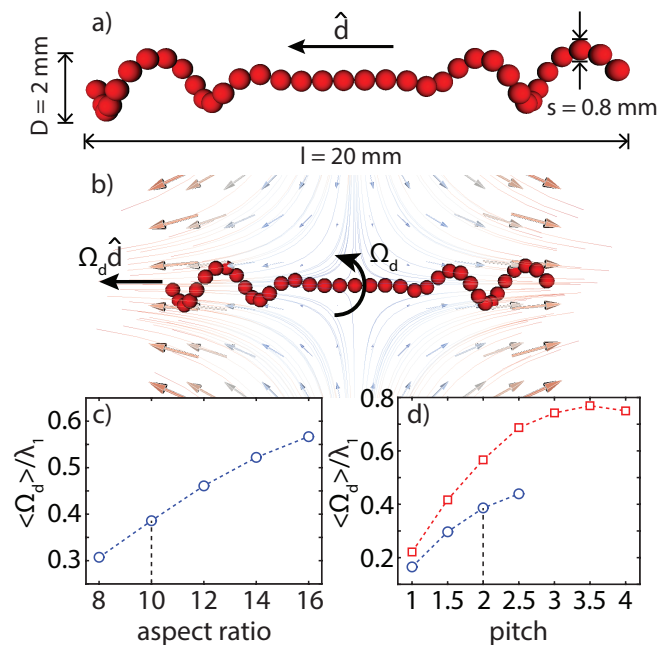


FIG. 1. (a) **Model of a chiral dipole made of 40 spheres.** The dipole vector \hat{d} points from right-handed helix to left-handed helix. (b) Response of a chiral dipole to a pure strain flow as indicated by the arrows. (c) Mean spinning rate $\langle \Omega_d \rangle$ as function of the overall aspect ratio, $\alpha = l/D$ (o: pitch = 2). (d) Mean spinning rate as function of helix pitch (o: $\alpha = 10$, \square : $\alpha = 16$). The mean spinning rate is measured in the Stokesian dynamics simulations and is normalized by the largest eigenvalue of the strain rate tensor λ_1

in this aligned state. Figure 1(c) shows that increasing the aspect ratio with constant pitch increases the spinning of a chiral dipole in a strain flow. Figure 1(d) shows the mean spinning rate as a function of pitch with constant aspect ratio and suggests that there is an optimal pitch near 3.5. This is consistent with the optimal pitch near π found for efficient propulsion by bacterial flagella [18]. So a particle with pitch near 3.5 and very high aspect ratio should yield the largest coupling of spinning to the strain rate.

The experiments were performed in a turbulent flow between oscillating grids [19]. The grids were driven in phase at a frequency of 1 Hz and 3 Hz in separate runs, resulting in a Taylor Reynolds number of $R_\lambda = 120$ and $R_\lambda = 183$, respectively. The parameters characterizing the turbulent flow are shown in Table I. We use 3D printing technology [20] to fabricate 2000 chiral dipoles with aspect ratio $\alpha = 10$, pitch 2 and a largest dimension of 20 mm, which corresponds to 35η and 72η , depending on the Reynolds number. This particle size places them in the inertial range of the turbulent flow. These dimensions were chosen because the 3D printers were not able to mass produce structurally stable particles with

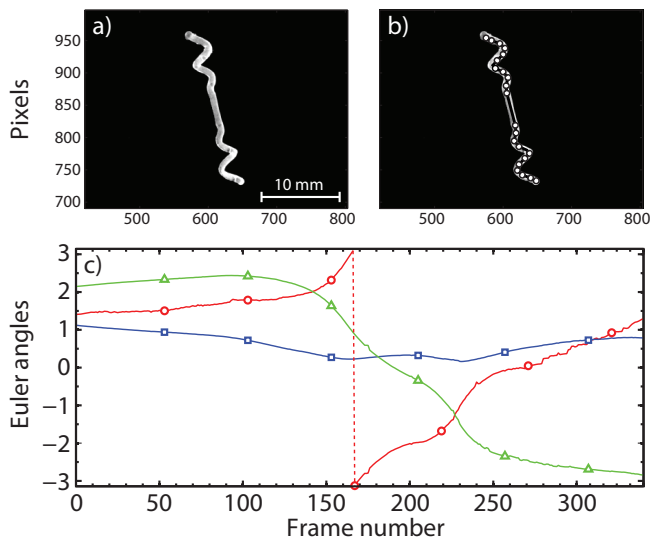


FIG. 2. (a) Cropped image of a chiral dipole from one camera. (b) Projection of the model onto the image plane of the camera using the measured Euler angles. (c) Time series of experimentally measured Euler angles ($\Delta = \phi$, $\square = \theta$, $\circ = \psi$) of a chiral dipole along its trajectory.

smallest dimension less than $s = 0.8$ mm, and we need $D \gg s$ in order to allow optical reconstruction of the particle's 3D orientation. Spherical tracer particles with a diameter of $150 \mu\text{m}$ were used to measure the rms fluid velocity and to calculate the third order longitudinal structure functions from which we determine the energy dissipation rate. **In order for the chiral dipoles to be neutrally buoyant, the fluid was density was increased until $\rho = 1.20 \text{ g cm}^{-3}$, which resulted in a fluid viscosity of $\nu = 2.00 \text{ mm}^2 \text{ s}^{-1}$.** The particles are fluorescent and illuminated with laser beams from four directions to minimize self-shadowing [20]. Four cameras image the particles from different angles at a frame rate of 450 Hz.

Using the images and camera calibration parameters from all four cameras, we can measure the three Euler angles defining the orientation of the chiral dipole. This is done by projecting a computer generated, 3D model of the particle onto the image plane of each camera [21]. A non-linear least squares search finds an orientation of the 3D model that minimizes the difference between the four projections of the model and the four experimental images. **The model consists of 30 individual, rigidly connected rods as shown in Fig. 2(b).** Figure 2(c) shows the measured Euler angles along a typical trajectory. The full solid-body rotation vector can be measured by fitting the particles orientation over several time steps along individual trajectories. The algorithm for finding the Euler angles is quite stable with respect to small variations in the particle shape, and it can reject images of particles that are broken or have larger deviations in the particle shape. It also could be easily modified to measure other

TABLE I. Flow parameters: $R_\lambda = (15\bar{u}L/\nu)^{1/2}$ Taylor Reynolds number, $L = \bar{u}^3/\epsilon$ energy input length scale, $\bar{u} = (\langle u_i u_i \rangle / 3)^{1/2}$ rms-velocity, ϵ mean energy dissipation rate, $\eta = (\nu^3/\epsilon)^{1/4}$ Kolmogorov length scale, $\tau_\eta = (\nu/\epsilon)^{1/2}$ Kolmogorov time scale, $\nu = 2.00 \times 10^{-6} \text{ m}^2 \text{ s}^{-1}$ kinematic viscosity.

Experiments						
Grid freq. [Hz]	R_λ	L [mm]	\bar{u} [mm s $^{-1}$]	ϵ [mm 2 s $^{-3}$]	η [mm]	τ_η [s]
1	120	94	20.4	90	0.546	0.149
3	183	80	55.6	2150	0.247	0.030
Simulations						
N	R_λ	L	\bar{u}	ϵ	η	τ_η
2048	400	4.08	1.411	0.687	0.0028	0.0225

particles made of slender filaments.

In addition to the experimental measurements, we use direct numerical simulations (DNS) of homogenous isotropic turbulence at a Reynolds number of $R_\lambda = 400$ to calculate the motion of a chiral dipole along its trajectory. The simulation volume includes a total of $N^3 = 2048^3$ collocation points and $\mathcal{O}(10^7)$ measurements of velocity gradients along Lagrangian particle trajectories for a few large eddy turnover times [22]. The characteristic quantities of the simulations are summarized in Table I.

High aspect ratio chiral dipoles can be approximated by rods and their tumbling rate can therefore be described by Jeffery's equation [23]

$$\dot{d}_i = \Omega_{ij}d_j + \frac{\alpha^2 - 1}{\alpha^2 + 1}(S_{ij}d_j - d_i d_k S_{kl}d_l), \quad (1)$$

where S_{ij} (strain rate tensor) and Ω_{ij} (rotation rate tensor) are the symmetric and anti-symmetric parts of the velocity gradient tensor, respectively. We can use the velocity gradients from the DNS to integrate Jeffery's equation and obtain the orientation valid for a particle in the dissipation range that has been aligned by the flow. **Equation (1) is only an approximation for chiral dipoles.** Marcos *et al.* [24] showed that chiral particles in shear flow experience a translational motion along the velocity gradient. Two opposite chiral centers that are spatially separated should show no cross-stream translational motion, but this same mechanism should produce a small torque. **For our large aspect ratio chiral dipoles, this torque is negligible compared to the torques captured by Jeffery's equation.**

In addition to tumbling, a thin rod is also spinning around its symmetry axis with half of the fluid vorticity ω in that direction. Chiral dipoles have an additional contribution to their spinning rate from the strain flow,

so we model the chiral dipole spinning rate with

$$\Omega_d = \frac{\omega_i}{2} d_i + \beta d_i S_{ij} d_j \quad (2)$$

$$= A_S + \beta A_L \quad (3)$$

The constant β is strongly dependent on the particle shape and describes the strength of the coupling of the spinning rate to the strain field. An approximate value for β for our particle shape was obtained from the Stokesian dynamics simulations, where $\beta = 0.39$. This value of β is only valid for small particles since it assumes Stokes flow around the particles. We adopt the compact notation developed for the analysis of the ‘advected delta-vee’ system by Li and Meneveau [6, 7] to define the longitudinal and transverse velocity gradients with respect to the particle. The longitudinal component is $A_L = d_i S_{ij} d_j$ and the transverse component is the magnitude of the tumbling rate $A_N = (d_i d_i)^{1/2}$. We can complete the picture if we include the spinning due to the fluid vorticity $A_S = \frac{1}{2} \omega_i d_i$. In Eq. 3, the instantaneous spinning rate depends on both the material element stretching rate A_L , and the vorticity component along the particle axis, A_S . Because a chiral dipole is equally likely to be parallel or anti-parallel to the vorticity vector, the mean spinning due to vorticity is zero, and so the mean value of A_L can be measured directly from $\langle A_L \rangle = \langle \Omega_d \rangle / \beta$.

Figure 3(a) shows the probability density function (PDF) of the spinning rate from both experimental measurements and the simulations. The PDFs collapse surprisingly well given the fact that the experiments were performed with particles in the inertial range and the simulations are for particles in the dissipation range. There is a clear asymmetry around zero in both the experimental and simulation data. The larger probability of positive spinning rate demonstrates the preferential rotation of chiral dipoles advected in isotropic turbulence. In the simulations, we can separate the contributions from strain and vorticity as shown in Fig. 3(b). Since the mean contribution from vorticity is zero, the contribution from the strain is responsible for the non-zero mean spinning rate. In addition to the mean, the PDFs show a strong positive skewness, $S = \langle (\Omega_d - \langle \Omega_d \rangle)^3 \rangle / \langle \Omega_d^2 \rangle^{3/2}$. For the experiments, $S = 1.1$ at $R_\lambda = 120$ and $S = 1.0$ at $R_\lambda = 183$. For the simulations, $S = 0.27$. The skewness reflects both the skewness of the longitudinal velocity differences in the 4/5 law and the complex dynamics of preferential alignment of slender bodies with vorticity and strain in turbulent flows. The larger skewnesses in the experiments compared with the simulation are not fully understood, but are likely to be partly a result of the much larger size of the chiral dipoles in the experiments.

The shape of the experimentally measured PDFs in Fig. 3(a) depends on the fit length, which is the number of time steps used when extracting the solid body rotation rate from the orientation measurements. Shorter fit lengths include more noise from the orientation measure-

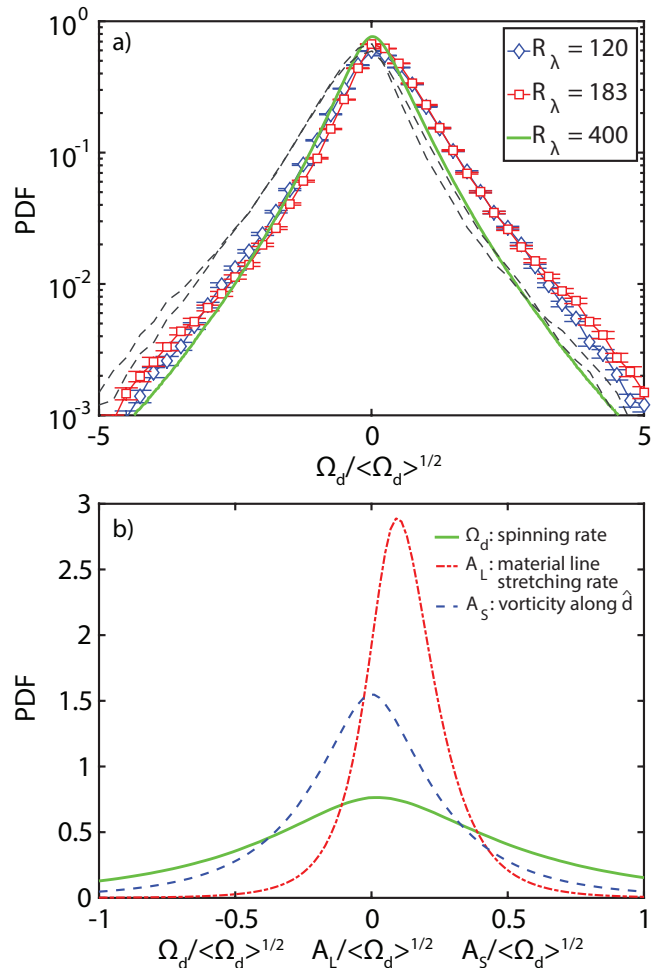


FIG. 3. (a) Probability density function (PDF) of the spinning rate Ω_d normalized by the standard deviation for both Reynolds numbers (blue \diamond , $R_\lambda = 120$ and red \circ , $R_\lambda = 183$) and simulations (green solid line). The gray dashed line shows experimental data mirrored around 0. (b) PDF of the individual contributions from strain, $A_L = d_i S_{ij} d_j$ (red dashed-dotted line) and vorticity, $A_S = \frac{1}{2} \omega_i d_i$ (blue dashed line) to the spinning rate Ω_d (solid green line). The standard deviation of the simulations is $\langle \Omega_d^2 \rangle^{1/2} = 0.85 \tau_\eta^{-1}$.

ments, leading to larger tails, whereas longer fit lengths filter out events of large rotational acceleration. Both experimental curves in Fig. 3 have been measured with a fit length of $0.5 \tau_\eta$.

The results from the DNS show a mean spinning rate of $\langle \Omega_d \rangle = 0.047 \tau_\eta^{-1}$. This is in agreement with the previously measured material line stretching rate $\zeta = 0.12 \tau_\eta^{-1}$ since $\langle \Omega_d \rangle = \beta \zeta$. The experimentally measured mean spinning rate is $\langle \Omega_d \rangle = 0.170 \pm 0.005 \tau_l^{-1}$ ($\langle \Omega_d \rangle = .26 \pm 0.01 \tau_l^{-1}$) for $R_\lambda = 120$ ($R_\lambda = 183$) normalized by $\tau_l = \frac{1}{\sqrt{15}} \frac{l}{u_l}$, where $u_l = \langle (\Delta u_l)^2 \rangle^{1/2}$ is the magnitude of the longitudinal velocity difference at separation l . The eddy turn-over time at scale l is chosen so that $\tau_l \rightarrow \tau_\eta$ for $l \rightarrow \eta$. A simple scaling law with the

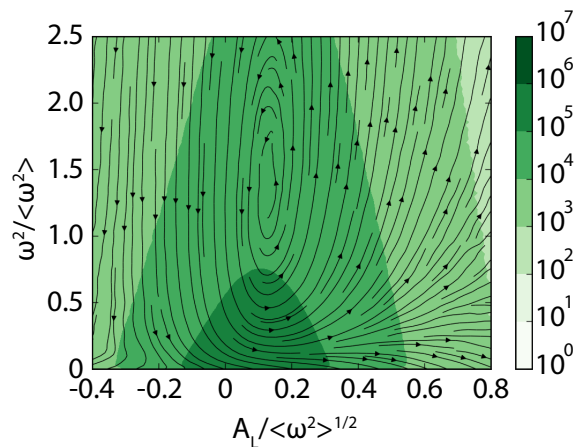


FIG. 4. Mean trajectories are representing the cyclic behavior of fluid elements in the phase space spanned by enstrophy, ω^2 and material line stretching rate A_L from the DNS. The color map shows the PDF.

mean spinning rate scaling with the eddy turn-over time at scale l does not hold. The larger than expected spinning rate of the larger chiral dipoles may be explained by two factors. First, the preferential alignment between the particle orientation and the extensional eigenvectors of the coarse grained strain rate tensor likely depends on particle size. Lüthi *et al.* [25] measured the coarse grained velocity gradient tensor and showed that the preferential alignment of vorticity moves toward the maximum extensional eigenvector as the coarse graining length scale increases. Second, the coupling constant β may depend on the particle Reynolds number so that chiral dipoles spin more efficiently in a turbulent environment than in the Stokes flow limit. Future work using numerical simulations of particles with lengths in the inertial range and experiments using particles with lengths at the Kolmogorov scale could clarify how the crossover from dissipation to inertial range scales affects the rotations of chiral dipoles.

The ability to follow elongated particles through the flow and observe the preferential stretching they experience suggests new ways to quantify the dynamic processes of the cascade. Figure 4 shows the mean trajectories of fluid elements in the space of enstrophy, ω^2 , and the material line stretching rate, A_L . There is a clear cyclical pattern with a fixed point at large enstrophy and a positive value of the material line stretching rate. A qualitatively similar cycle has been observed for the vortex stretching process by Ooi *et al.* [10] reflecting the similar physics involved in vortex stretching and material line stretching.

Chiral dipoles experience a preferential rotation direction in isotropic turbulence. The ability to fabricate particles with complex shapes and measure their rotational

motion opens the door to the study of a wide variety of particle shapes beyond the axisymmetric ellipsoids that have been the focus of most previous work. The mechanism of the preferential rotation is alignment of the slender particles by the fluid strain at the scale of the particle so that the particles experience extensional strain on average which produces preferential rotation due to the chiral ends. These measurements highlight the importance of analyzing turbulent flows in an oriented Lagrangian reference frame [6, 7]. Future work is needed to clarify the scale dependence of preferential alignment and rotation. Study of coarse grained rotation and deformation have yielded substantial insights into the dynamics of turbulence [25, 26]. Our current experiments and simulations show partial agreement in the shape of the spinning rate PDF, but the experiments are limited to inertial range particle sizes and the simulations are limited to dissipation range particle sizes. Tools to measure and simulate particles across the full range of turbulent scales could provide a powerful new way to analyze the dynamics of the turbulent cascade process.

We acknowledge support from NSF grants DMR-1208990 and DMR-1508575 as well as COST Actions MP0806, MP1305 and FP1005. We thank Brendan Cole for assistance with data acquisition, and Guy Geyer Marcus, Rui Ni, Tom Powers, and Luca Biferale for stimulating discussions.

* gvoth@wesleyan.edu; <http://gvoth.research.wesleyan.edu/>

† f.toschi@tue.nl; <http://toschi.phys.tue.nl/wordpress/>

- [1] G. K. Batchelor, Proc. R. Soc. A **213**, 349 (1952).
- [2] S. S. Girimaji and S. B. Pope, J. Fluid Mech. **2202**, 427 (1990).
- [3] S. Goto and S. Kida, J. Fluid Mech. **586**, 59 (2007).
- [4] M. Byron, J. Einarsson, K. Gustavsson, G. A. Voth, B. Mehlig, and E. Variano, Phys. Fluids **27**, 035101 (2015).
- [5] J. P. Salazar and L. R. Collins, Ann. Rev. Fluid Mech. **41**, 405 (2009).
- [6] Y. Li and C. Meneveau, Phys. Rev. Lett. **95**, 164502 (2005).
- [7] Y. Li and C. Meneveau, J. Fluid Mech. **558**, 133 (2006).
- [8] W. Ashurst, W. Kerstein, R. Kerr, and C. Gibston, Phys. Fluids **30**, 2343 (1987).
- [9] A. Tsinober, L. Shtilman, and H. Vaisburd, Fluid Dyn. Res. **21**, 477494 (1997).
- [10] A. Ooi, J. Martin, J. Soria, and M. S. Chong, J. Fluid Mech. **381**, 141 (1999).
- [11] A. Pumir and M. Wilkinson, New J. Phys. **13**, 093030 (2011).
- [12] S. Parsa, E. Calzavarini, F. Toschi, and G. A. Voth, Phys. Rev. Lett. **109**, 134501 (2012).
- [13] K. Gustavsson, J. Einarsson, and B. Mehlig, Phys. Rev. Lett. **112**, 014501 (2014).
- [14] R. Ni, S. Kramel, N. T. Ouellette, and G. A. Voth, J. Fluid Mech. **766**, 202 (2015).
- [15] R. Ni, N. T. Ouellette, and G. A. Voth, J. Fluid Mech.

- 743**, R3 (12 pages) (2014).
- [16] E. M. Purcell, Proc. Natl. Acad. Sci. USA **94**, 1130711311 (1997).
- [17] J. F. Brady and G. Bossis, Ann. Rev. Fluid Mech. **20**, 111 (1988).
- [18] S. E. Spagnolie and E. Lauga, Phys. Rev. Lett. **106**, 058103 (2011).
- [19] D. B. Blum, S. B. Kunwar, J. Johnson, and G. A. Voth, Phys. Fluids **22**, 015107 (2010).
- [20] G. G. Marcus, S. Parsa, S. Kramel, R. Ni, and G. A. Voth, New J. Phys. **16**, 102001 (2014).
- [21] B. C. Cole, G. G. Marcus, S. Parsa, S. Kramel, R. Ni, and G. A. Voth, J. Vis. Exp. **e53599**, doi:10.3791/53599 (2016).
- [22] R. Benzi, L. Biferale, E. Calzavarini, D. Lohse, and F. Toschi, Phys. Rev. E **80**, 066318 (2009).
- [23] G. B. Jeffery, Proc. R. Soc. A **102**, 715 (1922).
- [24] Marcos, H. C. Fu, T. R. Powers, and R. Stocker, Phys. Rev. Lett. **102**, 158103 (2009).
- [25] B. Lüthi, S. Ott, J. Berg, and J. Mann, J. Turbulence **8**, N45 (2007).
- [26] H. Xu, A. Pumir, and E. Bodenschatz, Nature Physics **7**, 709712 (2011).